The Energetics and Propagation Dynamics of Tropical Summertime Synoptic-Scale Disturbances

KAI-HON LAU*

Atmospheric and Oceanic Sciences Program, Princeton University, Princeton, New Jersey

NGAR-CHEUNG LAU

Geophysical Fluid Dynamics Laboratory/NOAA, Princeton University, Princeton, New Jersey

(Manuscript received 15 November 1991, in final form 21 February 1992)

ABSTRACT

Periods of enhanced synoptic activity in the tropical western Pacific, Bay of Bengal–northeastern India, and African–Atlantic regions are identified by extended empirical orthogonal function analysis. Composite meteorological fields for such active periods at various sites are constructed using European Centre for Medium-Range Weather Forecasts (ECMWF) analyses for the northern summers of 1980–1987. These composite data form the basis for evaluating the contributions of different dynamical processes to local balances of heat, moisture, vorticity, enstrophy, and energy, so that the propagation dynamics and principal energy sources of the tropical disturbances may be studied in detail.

In all three tropical regions considered here, the westward propagation of the synoptic-scale disturbances is attributed mostly to vorticity advection by both the time-mean flow and the transient fluctuations.

In the western Pacific and Indian sectors, condensation heating associated with cumulus convection is seen to be the most significant energy source for the tropical disturbances. The stretching effect associated with large-scale convective activity is the most important mechanism for the generation of eddy enstrophy in these maritime disturbances. There is substantial barotropic conversion of enstrophy and kinetic energy from the time-mean flow to the transient fluctuations.

In the African–Atlantic sector, the disturbances along the more prominent northern track at approximately 20°N are accompanied by dry desert-type convection. Vortex stretching associated with the dry convection is still the most important process for the generation of eddy enstrophy in these disturbances. However, the main source of available potential energy for these North African disturbances is the baroclinic conversion from the time-mean flow to the transient fluctuations along the zone of strong temperature gradients south of the Sahara. The dynamics and energetics of the weaker southern disturbances along 10°N in the African–Atlantic sector are similar to the moist disturbances found in the western Pacific and Indian sectors.

1. Introduction

As compared to our knowledge of midlatitude baroclinic waves, the current understanding of tropical synoptic-scale disturbances is more limited. One of the difficulties encountered in the study of tropical disturbances is the lack of reliable data coverage over extensive oceanic areas where such disturbances reside. Before the 1980s, our database for empirical studies of tropical disturbances was confined mostly to observations taken during short-term, limited-domain field experiments, or to rawinsonde records from stations located in western Pacific, western Africa, and the Caribbean islands. These data records have provided significant insights in the characteristics of disturbances in different tropical regions [see, e.g., Reed and Recker (1971), Burpee (1972, 1974), Reed et al. (1977), Shapiro (1986), and many others]. However, it still has been rather difficult to form a comprehensive picture of the nature of synoptic-scale activity in the entire tropical zone, partly because of variations in the length of data records and analysis techniques in different studies, and partly due to the sparsity of observations in some tropical regions (e.g., the eastern Pacific).

The first comprehensive dataset for the study of tropical disturbances is the observations gathered during the First GARP (Global Atmospheric Research Program) Global Experiment (FGGE). Using July and August wind and outgoing longwave radiation (OLR) data for the FGGE year, Nitta et al. (1985) and Nitta and Takayabu (1985) documented the characteristics of summertime disturbances in the northern tropics

* Present affiliation: The Joint Institute for the Study of the Atmosphere and Ocean, University of Washington, Seattle, Washington.

Corresponding author address: Dr. Kai-Hon Lau, University of Washington, Joint Institute for the Study of the Atmosphere and Ocean GJ-40, Seattle, WA 98195.

during 1979. After the FGGE year, the daily accumulation of global analysis products at various operational centers has significantly expanded the database for more extensive observational studies of tropical disturbances. In a recent paper, Lau and Lau (1990; hereafter referred to as LL) documented the structure and propagation characteristics of summertime tropical disturbances using an eight-year record of the operational analyses produced at the European Centre for Medium-Range Weather Forecasts (ECMWF). It was demonstrated that various key findings on tropical disturbances reported in earlier studies could readily be reproduced using this modern dataset, and that a considerable amount of new information on these disturbances could be extracted from the global analysis products.

The sites of strong synoptic-scale activity during the northern summer, as identified in Nitta et al. (1985) and LL, include the western Pacific, the Bay of Bengal–northeastern India, the eastern Pacific, and the western Africa–Atlantic–Caribbean regions. Lau and Lau (1990) found dominant spectral peaks with periods ranging from 3 to 8 days at the active sites. Using lag-correlation and regression statistics, they documented the horizontal structure, propagation characteristics, and growth–decay rates of the 850-mb synoptic-scale vorticity fluctuations. Typical periods, wavelengths, and phase speeds of the tropical disturbances occurring in various regions are summarized in Table 1 of LL. The tropical disturbances tend to travel westward or northwestward, with the upstream and downstream portions of each preferred propagation path being characterized by growth and decay in eddy amplitude, respectively.

Lau and Lau (1990) applied an extended empirical orthogonal function (EEOF) analysis to identify the dominant synoptic-scale fluctuations in the western Pacific, Indian, and African–Atlantic sectors. The three-dimensional structure of selected meteorological variables associated with the principal modes was described using a compositing procedure based on the time coefficients of the leading EEOFs. With these composites, the roles of various dynamical processes were inferred *qualitatively* by noting the phase relationships among different variables, and also by the positioning of various circulation features relative to the quasi-stationary flow field. These inferences are similar to those made in previous investigations. For example, the coincidence of warm, rising motion in the upper troposphere with negative OLR perturbations (i.e., high cloud tops) is suggestive of the importance of latent heat release accompanying moist convection (e.g., Wallace and Chang 1969; Reed and Recker 1971), whereas the horizontal phase tilts of the vorticity fluctuations and their placement with respect to the quasi-stationary circulation are indicative of barotropic transfer of kinetic energy from the mean flow to the transient fluctuations (Reed et al. 1977). Variations in eddy structure in association with different environments were also identified in LL. A notable example is the African disturbances found along 20°N near the zone of strong meridional temperature gradient south of the Sahara Desert. The characteristics of these disturbances are similar to those of thermal lows, with dry, warm, rising motion above the wave troughs, and relatively moist, cool, sinking motion above the ridges. These properties suggest that dry convection plays a significant role in the northern African disturbances (Burpee 1972, 1974). Most of the studies cited here are rather descriptive in nature, whereas *quantitative* estimates of the relative importance of the various dynamical processes in tropical disturbances are more limited. Norquist et al. (1977) used a compositing method to study the energy budget of African disturbances, and found that baroclinic and barotropic processes contribute almost equally to the generation and maintenance of these disturbances. By making use of the mean and eddy composite fields obtained in LL, we shall conduct similar budget studies to enhance our understanding of the dynamics of the tropical disturbances.

The present study is a continuation of our investigation on tropical transient fluctuations started in LL based on gridded fields from ECMWF. The EEOF compositing method in LL conveniently yields a full four-dimensional description of the space–time evolution of any variable for the tropical disturbances occurring in different active regions. We shall henceforth use these composite fields to examine the manner in which the transient fluctuations participate in various dynamical processes. Specifically, we shall evaluate the local balances of heat, moisture, vorticity, enstrophy, and kinetic and available potential energy for the tropical transient modes. The results presented here complement those already reported in LL in offering a detailed documentation of the nature of tropical disturbances during the northern summer. These findings should in turn facilitate further investigations of the role of synoptic-scale transient fluctuations in the general circulation of the tropical atmosphere.

In the next section, we shall briefly describe the dataset, the EEOF analysis, and the compositing procedures. Many earlier studies have identified condensation heating as the most important energy source for transient fluctuations over the tropical oceans. Hence, to clarify the role of latent heating and the relative importance of different diabatic processes associated with the disturbances, we shall first examine the local heat and moisture budgets of the principal tropical modes in section 3. On the other hand, the evidence presented in LL indicates that dry convection prevails in disturbances found near the zone of strong meridional temperature gradient south of the Sahara desert, thus suggesting that the eddies may be extracting available potential energy from the mean temperature gradient in that region. To ascertain the importance of

the latter mechanism, an approximate eddy available potential energy balance will also be examined in section 3. We shall then proceed to analyze the local vorticity balance of the disturbances in section 4, so as to study the processes responsible for the propagation and growth of the vorticity fluctuations. The local balances of two second-order eddy quantities, eddy enstrophy and eddy kinetic energy, will be studied in section 5. The eddy-enstrophy budget provides a rather concise description of the maintenance of the rotational part of the wind field in the disturbances. The significance of the irrotational part of the fluctuations will then be discussed as part of the eddy kinetic energy budget. Key results will be summarized in the final section.

2. Dataset and EEOF composites

The dataset and EEOF compositing procedures are the same as in LL, and will be described here only briefly. The reader is referred to LL for a more detailed discussion. The primary dataset consists of the ECMWF operational analyses for the 1980–1987 June, July, and August (JJA) period. The variables include zonal and meridional wind u and v, pressure velocity ω, temperature T, geopotential height Z, and specific humidity q. Data are available twice daily at seven standard pressure levels from 1000 to 100 mb. Specific humidity is available only up to the 300-mb level. When necessary, the value of q at 100 and 200 mb is assumed to be zero in the budget calculations.

To focus our attention on regions with strong synoptic-scale activity, three domains are chosen for detailed analyses: namely, the western Pacific and Indian (10°S–40°N, 60°E–180°), the Atlantic (15°S–30°N, 90°W–30°E), and the eastern Pacific (10°S–40°N, 165°–75°W) domains. Dominant modes of synoptic-scale fluctuations in these domains are identified from pairs of leading EEOFs or rotated EEOFs (REEOFs) of the bandpass-filtered time series of 850-mb vorticity ζ. (In EOF analysis, propagating phenomena are often represented by paired modes with comparable fractions of explained variance, and in quadrature with one another both temporally and spatially.) The digital bandpass filter has half-power points at 2.5 and 12.5 days, and full response for periods from 3 to 10 days.

For each of the principal modes, the amplitude $A(t)$ and phase $\theta(t)$ are defined from time coefficients $C_1(t)$ and $C_2(t)$ of the paired EEOFs/REEOFs (see LL, Fig. 13), as:

$$A(t) = \left[\frac{C_1^2(t) + C_2^2(t)}{2}\right]^{1/2} \quad \text{and}$$

$$\theta(t) = \tan^{-1}\left[\frac{C_2(t)}{C_1(t)}\right].$$

The space–time evolution of any variable (say, ζ) associated with a certain characteristic mode is described by forming composites of ζ at eight individual phases θ_i, which vary in equal increments of 45° (i.e., one-eighth of a phase cycle). The composites, denoted as $\zeta(\theta_i)$, are obtained by averaging ζ over those times corresponding to the same phase θ_i of selected strong episodes. Strong episodes are defined as time intervals during which the phase $\theta(t)$ evolves through at least one complete cycle, and the amplitude $A(t)$ is larger than a certain threshold (0.75 standard deviation). The reader is referred to section 6 of LL for more details of the compositing procedure.

In LL, the structure of transient disturbances in different active sites was illustrated by composites based on *bandpass-filtered* data fields. In the present study, magnitudes of both the *time-mean* and *fluctuating* parts of the variables are needed to evaluate the relative contributions of different dynamical processes. Therefore, composites of all variables used in this study are derived from the *unfiltered* data fields. We shall henceforth denote the *fluctuating* component in any variable (say, ζ) at phase θ_i as

$$\zeta'(\theta_i) \equiv \zeta(\theta_i) - \bar{\zeta},$$

where $\overline{(\ )}$ denotes a time average over all eight phase composites $\zeta(\theta_i)$ of the corresponding unfiltered variable. The phase average defined here, $\bar{\zeta}$, is interpreted as the *time-mean state* of ζ when the transient fluctuations are active. The structure of the bandpass-filtered phase composites (in LL) is almost identical to that of the fluctuating component derived from the corresponding unfiltered time series, and their amplitudes generally differ by less than 20%–30%.

Composites of the time-mean and fluctuating components for the variables u, v, ω, Z, T, q, and ζ are constructed for the western Pacific (WP), Indian (IN), and African–Atlantic (AT) modes. These composite fields will be used to examine the various budgets of the transient fluctuations in the following sections. As in LL, we shall describe the WP disturbances in greater detail, and mention only those aspects of the IN and AT disturbances that are significantly different from the WP mode. More detailed descriptions of the budgets for each of the three active regions can be found in Lau (1991).

3. Diabatic heating and eddy available potential energy balance

In LL, large positive (negative) temperature anomalies were seen to be coincident with rising (sinking) eddy motion in the upper troposphere for the WP and the IN disturbances, and in the lower troposphere for the northern AT disturbances (see LL, Figs. 16, 20, and 23). This phase relationship yields $-\overline{\omega'T'} > 0$, which implies a conversion of eddy available potential energy (EAPE) to eddy kinetic energy (EKE). The EAPE being converted to EKE has to be replenished by other mechanisms, such as *condensation heating* (Wallace and Chang 1969; Carlson 1969a,b) or *baroclinic conversion* from mean available potential energy

(MAPE) (Burpee 1972, 1974; Norquist et al. 1977). These mechanisms will be examined in this section. We shall first assess the significance of various diabatic heating processes by comparing the residuals of the heat and moisture budgets for the transient disturbances (i.e., the apparent heat source and moisture sink). The relative importance of diabatic and baroclinic processes in the generation of EAPE for the tropical disturbances will then be analyzed using an approximate EAPE balance equation.

a. Apparent heat source and moisture sink

Following Nitta (1972) and Yanai et al. (1973), we define the apparent heat source Q_1 and apparent moisture sink Q_2 as residuals of the thermodynamic and moisture equations:

$$Q_1 \equiv c_p\left(\frac{p}{p_0}\right)^{\kappa}\frac{D\Theta}{Dt} = c_p\frac{\partial T}{\partial t} - c_p(\omega\sigma - \mathbf{V}_h\cdot\nabla_h T) \quad (1a)$$

$$Q_2 \equiv -L\frac{Dq}{Dt} = -L\frac{\partial q}{\partial t} - L\mathbf{V}_h\cdot\nabla_h q - L\omega\frac{\partial q}{\partial p}, \quad (1b)$$

where c_p is the specific heat at constant pressure, $p_0 = 1000$ mb, $\kappa \equiv R/c_p$, Θ the potential temperature, $\mathbf{V}_h$ the horizontal velocity vector, ∇_h the horizontal gradient operator, L the latent heat of condensation, $\sigma \equiv (RT/c_p p) - (\partial T/\partial p)$ the static stability, and R the gas constant. Furthermore, we define the vertical average, $\langle A\rangle$, and vertical integral, $\langle\langle A\rangle\rangle$, for any variable $A(p)$ as

$$\langle A\rangle \equiv \frac{1}{p_0 - p_t}\int_{p_t}^{p_0} A(p)dp \quad \text{and}$$

$$\langle\langle A\rangle\rangle \equiv \frac{1}{g}\int_{p_t}^{p_0} A(p)dp = \frac{p_0 - p_t}{g}\langle A\rangle,$$

where $p_t = 100$ mb. In this formulation, $\langle\langle Q_1\rangle\rangle$ can be interpreted as the sum of various diabatic heating terms, and $\langle\langle Q_2\rangle\rangle$ can be interpreted as the net moisture sink; that is,

$$\langle\langle Q_1\rangle\rangle \approx LP + \langle\langle Q_R\rangle\rangle + S \quad (2a)$$

$$\langle\langle Q_2\rangle\rangle \approx LP - LE, \quad (2b)$$

where P, E, Q_R, and S are the rates of precipitation, evaporation, radiative heating, and heating due to sensible heat flux through the lower boundary, respectively. If the diabatic heating is dominated by latent heat release due to condensation (i.e., $LP \gg LE$, S, or $\langle\langle Q_R\rangle\rangle$), the distributions of $\langle\langle Q_1\rangle\rangle$ and $\langle\langle Q_2\rangle\rangle$ are expected to be similar. Hence, the importance of condensation heating may be inferred indirectly by comparing the horizontal distributions of Q_1 and Q_2 (Yanai et al. 1973). Furthermore, since different condensation processes (e.g., cumulus convection and continuous frontal rain) are associated with distinctive vertical profiles of Q_1 and Q_2, the nature of the dominant condensation process may also be inferred by examining the vertical distributions of Q_1 and Q_2 in regions in which latent heating is important [see Yanai et al. (1973) and Luo and Yanai (1984) for more details].

To analyze the diabatic heating field associated with the *transient fluctuations,* we derive the appropriate *perturbation* thermodynamic and moisture equations by first taking the phase average of (1), and then subtracting the results from the original equations. We obtain

$$Q_1' = c_p\frac{\partial T'}{\partial t} - c_p(\omega'\bar{\sigma} - \mathbf{V}_h'\cdot\nabla_h\bar{T}) - c_p(\bar{\omega}\sigma' - \overline{\mathbf{V}_h}\cdot\nabla_h T') - c_p(\omega'\sigma' - \mathbf{V}_h'\cdot\nabla_h T')' \quad (3a)$$

$$Q_2' = -L\frac{\partial q'}{\partial t} - L\left(\mathbf{V}_h'\cdot\nabla_h\bar{q} + \omega'\frac{\partial\bar{q}}{\partial p}\right) - L\bar{\mathbf{V}}\cdot\nabla q' - L(\mathbf{V}'\cdot\nabla q')', \quad (3b)$$

where $\mathbf{V}$ is the three-dimensional velocity vector, and ∇ the three-dimensional gradient operator.

Using composites of the time mean and fluctuating temperature, humidity, and motion fields derived from the unfiltered time series (section 2), the terms on the right-hand side of (3) can be evaluated at any phase θ_i of the eddy cycle. [The local time rate of change of any variable at any phase is estimated by a centered time difference, with the time interval between successive phases being approximated as one-eighth of the average period estimated for the corresponding EEOF–REEOF mode (LL, Table 1).] In analogy with (2), $\langle\langle Q_1'\rangle\rangle$ and $\langle\langle Q_2'\rangle\rangle$ are *interpreted* as the apparent heat source and moisture sink associated with the transient fluctuations:

$$\langle\langle Q_1'\rangle\rangle \approx LP' + \langle\langle Q_R'\rangle\rangle + S'$$

$$\langle\langle Q_2'\rangle\rangle \approx LP' - LE'.$$

Hence, the distributions of $\langle\langle Q_1'\rangle\rangle$ and $\langle\langle Q_2'\rangle\rangle$ are expected to be similar if the diabatic heating associated with the disturbances is dominated by latent heat release.

Vertically averaged distributions of Q_1' and Q_2' for the WP disturbances at phase $\theta_i = 90°$ are shown in Figs. 1a and 1b, respectively. (The phases of all parameters shown in this study are the same as those chosen to depict the characteristic structure of the corresponding transient mode in LL.) Inspection of the vertically averaged distributions of terms on the right-hand side of (3a) reveals that the net diabatic heating Q_1' in the WP disturbances is almost entirely balanced by the adiabatic cooling associated with the eddy vertical motion (i.e., $Q_1' \approx -c_p\omega'\bar{\sigma}$). Similarly, the net moisture loss Q_2' for the WP disturbances is largely balanced by

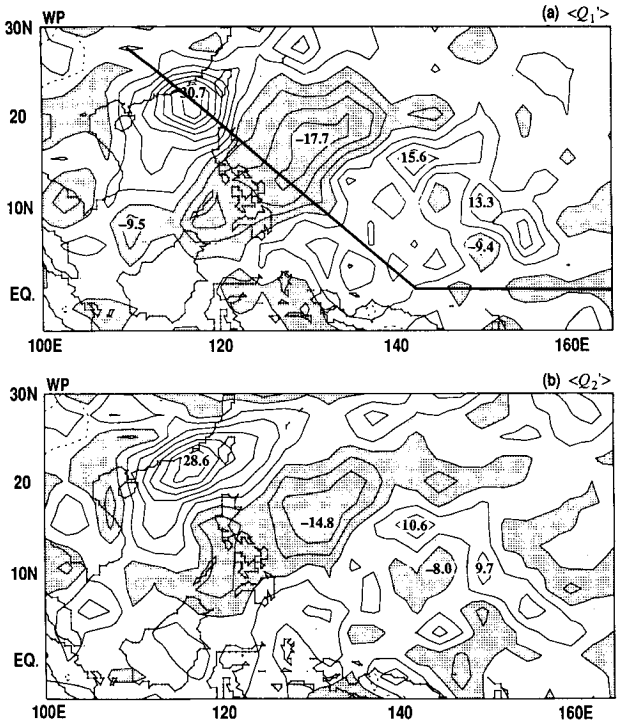

FIG. 1. Vertically averaged distributions of (a) Q_1' and (b) Q_2' for the WP disturbances at phase $\theta_i = 90°$. Contour interval is 4×10^{-3} m^2 s^{-3}. Stippling indicates negative values less than -2×10^{-3} m^2 s^{-3}. The values displayed here may be multiplied by $(p_0 - p_t)/g = 9174 \approx 10^4$ to yield estimates of $\langle\langle Q_1' \rangle\rangle$ and $\langle\langle Q_2' \rangle\rangle$ in watts per square meter.

the vertical advection of mean specific humidity by the transient eddies (i.e., $Q_2' \approx -L\omega' \partial \bar{q}/\partial p$). As discussed earlier, the similarity between $\langle Q_1' \rangle$ and $\langle Q_2' \rangle$ in Fig. 1 suggests that the dominant diabatic process associated with the WP disturbances is condensation heating, which is consistent with the observation that $\langle Q_1' \rangle$ and $\langle Q_2' \rangle$ exhibit a distinct out-of-phase relationship with the corresponding OLR fluctuations (LL, Fig. 14b).

Vertical cross sections of Q_1' and Q_2' are shown in Fig. 2. The abscissa corresponds to the mean propagation path of the WP disturbances, and extends from southern China (27.5°N, 110°E) in the extreme left to the western equatorial Pacific (2.5°N, 165°E) in the extreme right (the bold line in Fig. 1a). (The abscissa used for the WP mode vertical cross sections in this study is similar to its counterpart in LL, except for the eastward extension from 145° to 165°E along 2.5°N.) The extrema of Q_1' in the upper troposphere between 200 and 300 mb are directly related to the upper-level vertical-motion centers of the WP disturbances (LL, Fig. 16). In contrast, because of the much larger values of mean specific humidity in the lower troposphere, extrema of Q_2' are found between 700 and 850 mb in association with the low-level vertical motion centers. Since the moisture sink due to condensation (Q_2') should coincide with the latent heat release (Q_1'), the notable difference in the altitudes of the extremes of Q_1' and Q_2' (Fig. 2) implies that there must exist significant vertical transports of moisture and heat between the lower and upper troposphere that are not resolved in the ECMWF dataset or the compositing procedure. This vertical transport is usually attributed to subgrid-scale cumulus convection. [The reader is referred to Yanai et al. (1973) and Luo and Yanai (1984) for more detailed discussions and explanations of different vertical profiles of the apparent heat source and moisture sink.] Hence, in agreement with earlier studies by Wallace and Chang (1969), Reed and Recker (1971), and others, we conclude that condensation heating accompanying cumulus convection is the most important heat source for the WP disturbances. Since estimates of Q_1' and Q_2' as residuals in the heat and moisture equations are rather sensitive to the composite ω' field (Luo and Yanai 1984), and there are considerable uncertainties in the tropical vertical velocity and humidity fields in the ECMWF products (Trenberth and Olson 1988), the quantitative results described here must be viewed with caution. Further analyses using independent datasets should be performed to verify these findings.

General agreement between distributions of $\langle Q_1' \rangle$ and $\langle Q_2' \rangle$ is found for disturbances in the Indian monsoon region, and also for the AT disturbances along the southern propagation path (between 5° and 10°N and from 20°E to 45°W) and in the western Atlantic–Caribbean sector (along ~15°N, 60°–105°W). In the above regions, $\langle Q_1' \rangle$ and $\langle Q_2' \rangle$ are also out of phase with the corresponding OLR anomalies, and extremes

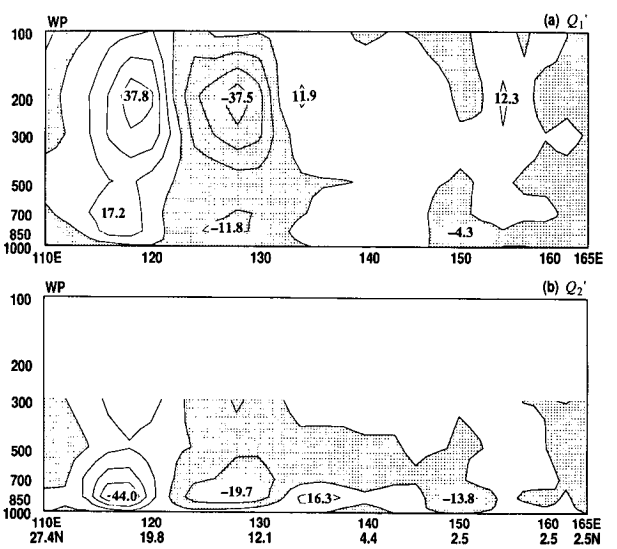

FIG. 2. Vertical cross sections of (a) Q_1' and (b) Q_2' for the WP disturbances. Contour interval is 10×10^{-3} m^2 s^{-3}. Stippling indicates negative values. The abscissa corresponds to the bold line segments in Fig. 1a.

of Q_1' appear directly above extremes of Q_2'. Comparatively larger differences between the horizontal distributions of $\langle Q_1' \rangle$ and $\langle Q_2' \rangle$ are found along the northern track of the AT disturbances near the Sahara Desert and the Africa–Atlantic coast ($\sim$20°E–10°W along 20°N), indicating that condensation heating does not dominate over other diabatic effects (S', LE', and $\langle\langle Q_R' \rangle\rangle$) in the latter areas. Moreover, we also note that the horizontal advection of mean temperature by the transient disturbances, $-c_p \mathbf{V}_h' \cdot \nabla_h \bar{T}$, is not negligible in the heat balance of the AT disturbances along the northern track. In the next subsection, we shall show that this finding has direct implications for the eddy available potential energy balance of the northern AT disturbances.

b. *Eddy available potential energy balance*

As described in the previous subsection, the heat balance of the tropical disturbances may be approximated by the equation:

$$Q_1' \approx c_p \frac{\partial T'}{\partial t} - c_p(\omega'\bar{\sigma} - \mathbf{V}_h' \cdot \nabla_h \bar{T}). \qquad (4)$$

In the western Pacific and Indian monsoon regions, Q_1' is almost entirely balanced by the $-c_p\omega'\bar{\sigma}$ term. The $-\mathbf{V}_h' \cdot \nabla_h \bar{T}$ term is important only for the AT disturbances, and particularly in the continental section along the northern track. We can form the following approximate equation for the EAPE of the tropical disturbances from (4):

$$\underbrace{\frac{\partial A_T}{\partial t}}_{\text{PT}} \approx \underbrace{-\frac{c_p\gamma}{\bar{T}} \overline{\mathbf{V}_h' T'} \cdot \nabla_h \bar{T}}_{\text{PI}} + \underbrace{\frac{R\overline{T'\omega'}}{p}}_{-\text{KP}} + \underbrace{\frac{\gamma \overline{Q_1' T'}}{\bar{T}}}_{\text{PQ}}, \qquad (5)$$

where $A_T \equiv c_p\gamma\overline{T'^2}/2\bar{T}$ is the EAPE (strictly speaking, EAPE is meaningful only in a vertically integrated sense), $\gamma \equiv \Gamma_d/(\Gamma_d - \Gamma)$, and Γ and Γ_d are the observed and the dry-adiabatic lapse rates, respectively. The term PT represents the time rate of change of EAPE. This term is identically zero, as EAPE is a phase-averaged quantity. The term PI describes the generation of EAPE through conversion from MAPE, and is positive when the eddy heat flux, $\overline{\mathbf{V}_h' T'}$, is directed down the mean temperature gradient $\nabla_h \bar{T}$. The second term on the right-hand side, $-$KP, represents the generation or destruction of EAPE through conversion from or to EKE. Positive values of KP indicate a conversion of EAPE to EKE through the rising (sinking) motion of warm (cold) air parcels. The last term, PQ, describes the generation of EAPE by diabatic effects as external heating (cooling) is applied to warm (cold) air parcels. A similar formulation of the EAPE balance was used by Norquist et al. (1977).

For the WP and IN disturbances, we find that the loss of EAPE through conversion to EKE, $-$KP, is mostly balanced by the generation of EAPE by external diabatic heating, PQ, and both processes are strongest in the mid- and upper troposphere. These results are expected since Q_1' is nearly equal to the $-c_p\omega'\bar{\sigma}$ term for the disturbances in these two regions. The balance between the PQ and KP terms implies that the mid- and upper-level diabatic heating due to cumulus convection is the dominant source of EAPE for the WP and IN disturbances.

Vertically averaged distributions of the PI, KP, and PQ terms for the AT disturbances are shown in Fig. 3, and the corresponding vertical cross sections are shown in Fig. 4. (The abscissa in Fig. 4 is the same as that used to depict the vertical structure of the northern AT disturbances in LL.) The distribution of $\langle \text{PI} \rangle$ shows large MAPE to EAPE conversion over the western Africa–eastern Atlantic sector, in the same region where strong EAPE to EKE conversion is observed (Figs. 3a and 3b). Both conversions (MAPE to EAPE, and EAPE to EKE) occur mainly in the lower troposphere (Figs. 4a and 4b). In comparison, the generation of EAPE by diabatic effects is much weaker (Figs. 3c and 4c). It is evident that the main balance of the EAPE budget for the northern AT disturbances is between the KP and PI terms, confirming that the strong loss of EAPE through conversion to EKE over the eastern Atlantic–western Africa is mostly maintained by the baroclinic conversion of MAPE to EAPE.

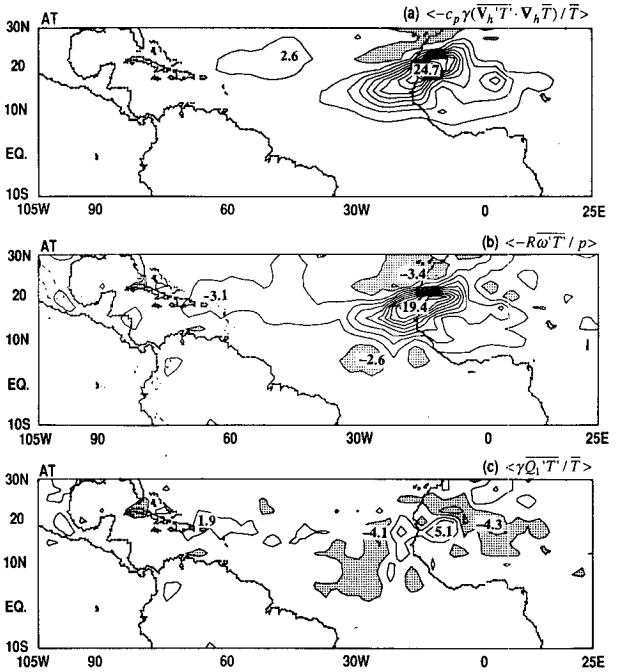

FIG. 3. Vertically averaged distributions of (a) $-c_p\gamma(\overline{\mathbf{V}_h'T'}\cdot\nabla_h\bar{T})/\bar{T}$, (b) $-R\overline{\omega'T'}/p$, and (c) $\gamma\overline{Q_1'T'}/\bar{T}$ for the AT disturbances. Contour interval is 2×10^{-6} m^2 s^{-3}. Stippling indicates negative values less than -1×10^{-6} m^2 s^{-3}.

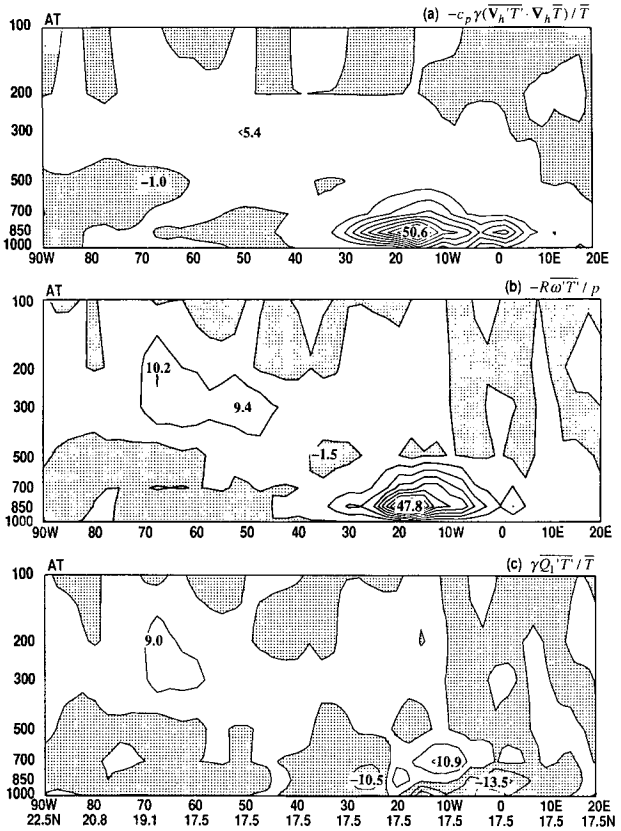

FIG. 4. Vertical cross sections of (a) $-c_p\gamma(\overline{\mathbf{V}_h'T'}\cdot\nabla_h\bar{T})/\bar{T}$, (b) $-R\overline{\omega'T'}/p$, and (c) $\gamma\overline{Q_1'T'}/\bar{T}$ for the AT disturbances. Contour interval is 5×10^{-6} m^2 s^{-3}. Stippling indicates negative values. The abscissa corresponds to the bold line segments in LL, Fig. 22a.

As noted earlier in this subsection, positive PI implies an eddy heat flux directed down the mean temperature gradient. From the 850-mb distribution of $\bar{T}$ in the African–Atlantic sector, we note that strong mean temperature gradients exist between the hot Sahara desert and the cooler eastern Atlantic and equatorial Africa. Apparently, the AT disturbances serve to transport heat away from the Sahara.

4. Perturbation-vorticity balance

Since the horizontal wind field in tropical disturbances is dominated by the rotational component, it is of interest to examine the maintenance and propagation dynamics of the vorticity fluctuations. We shall analyze the vorticity dynamics of the disturbances by studying the perturbation-vorticity balance in this section. The maintenance of the vorticity fluctuations will be examined in the context of the eddy enstrophy budget in the next section.

The perturbation-vorticity equation may be written as

$$\underbrace{\frac{\partial\zeta'}{\partial t}}_{\mathrm{VT}} = \underbrace{-\mathbf{V}'\cdot\nabla(\bar{\zeta}+f)}_{\mathrm{VA}_e} \underbrace{-\bar{\mathbf{V}}\cdot\nabla\zeta'}_{\mathrm{VA}_m} \underbrace{-(\mathbf{V}'\cdot\nabla\zeta')'}_{\mathrm{VA}_t} + \underbrace{\left[(f+\zeta)\frac{\partial\omega}{\partial p}\right]'}_{\mathrm{VD}} \underbrace{-\left(\mathbf{k}\cdot\nabla\omega\times\frac{\partial\mathbf{V}}{\partial p}\right)'}_{\mathrm{VC}} + \mathrm{VR} \quad (6)$$

where f is the Coriolis parameter, and $\mathbf{k}$ the vertical unit vector. The term VT represents the time rate of change of perturbation vorticity. The term VA_e denotes the advection of mean absolute vorticity by the transient fluctuations. This term can further be separated into the advection of mean relative vorticity by the transient fluctuations, $-\mathbf{V}'\cdot\nabla\bar{\zeta}$, and the beta effect, $-v'\beta = -(v'/a)(df/d\phi)$, where a is the earth radius and ϕ the latitude. The term VA_m describes the advection of vorticity fluctuations by the time-mean flow. Here, VA_t represents the fluctuating part of the nonlinear advection of perturbation vorticity by the transient fluctuations. The terms VD and VC describe the net vorticity tendency associated with stretching and tilting effects, respectively; VA_t and VC are negligible for all the EEOF modes we have analyzed, and will not be discussed any further in this study. For convenience, we shall refer to the sum of the first five terms on the right-hand side of (6) as VT_c. The last term VR is evaluated as the difference between VT and VT_c, and includes contributions from all processes not expressed explicitly in (6) (e.g., boundary friction, cumulus convection, and other subgrid-scale transports), as well as from cumulative errors in the estimates of various parameters in these balances.

Vertically averaged distributions of VT, VT_c, and VR at phase $\theta_i = 90°$ for the WP disturbances are shown in Fig. 5. It is evident that $\langle\mathrm{VT}_c\rangle$ agrees rather well with $\langle\mathrm{VT}\rangle$ over most of the region in which the WP disturbances are active. Both $\langle\mathrm{VT}\rangle$ and $\langle\mathrm{VT}_c\rangle$ exhibit a wavelike structure that lead $\langle\zeta'\rangle$ by about a quarter-wavelength. (To illustrate the phase relationships between the vorticity perturbations and the tendency terms, phase lines of $\langle\zeta'\rangle$ are shown as dash lines in Fig. 5.) We also note from distributions of $\langle\mathrm{VT}\rangle$ and $\langle\mathrm{VT}_c\rangle$ at other temporal phases that the agreement between $\langle\mathrm{VT}\rangle$ and $\langle\mathrm{VT}_c\rangle$ is rather good throughout the entire cycle of the WP mode. Figure 5c shows that $\langle\mathrm{VR}\rangle$ is small along the propagation path, except in the northwestern section near the south China coast, where strong decay of synoptic-scale activity was noted (LL, section 4d). Large negative values of $\langle\mathrm{VR}\rangle$ are found near the trough axis along the south China coast, indicating that $\langle\mathrm{VR}\rangle$ and $\langle\zeta'\rangle$ are almost 180° out of phase in this region. The negative VR at the wave trough may partly be a result of the frictional dissipation of the vorticity perturbations. The time scale

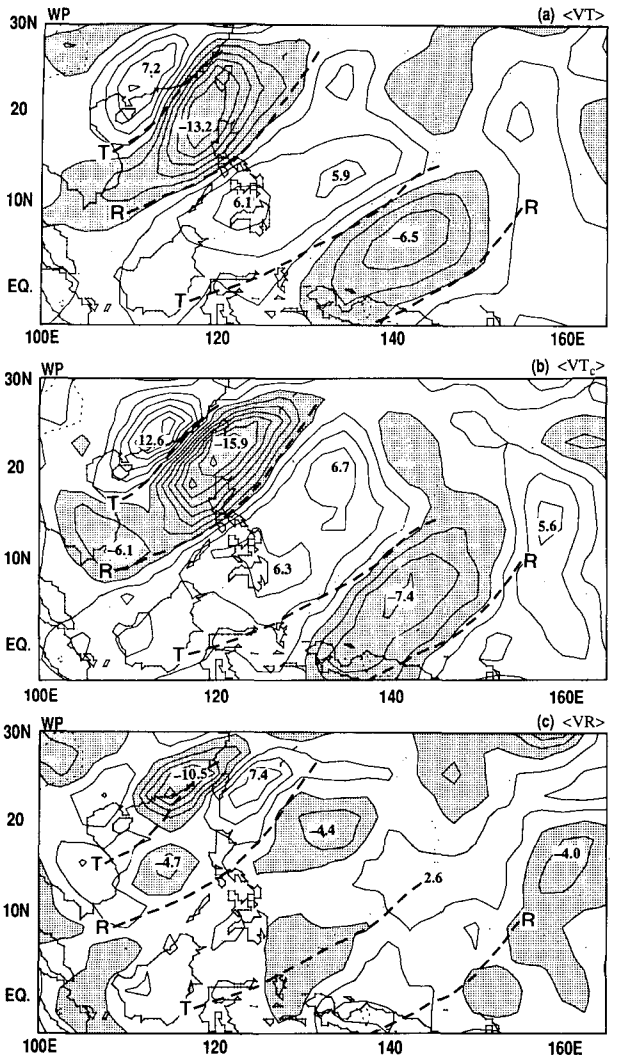

FIG. 5. Vertically averaged distributions of (a) VT, (b) VT_e, and (c) VR for the WP disturbances. Contour interval is 2×10^{-11} s^{-2}. Stippling indicates negative values less than -1×10^{-11} s^{-2}. The dash lines mark the trough (T) and ridge (R) axes of the vertically averaged WP vorticity fluctuations.

for dissipation near the south China coast, as estimated from the ratio $\langle \zeta' \rangle / \langle \mathrm{VR} \rangle$, is approximately 2 days.

The 850-mb distributions of the three most important terms in (6) contributing to VT_e of the WP disturbances are shown in Fig. 6 as (a) VA_e, (b) VA_m, and (c) VD. Since low-level convergence is usually accompanied by upper-level divergence, and vice versa, the column-averaged stretching term $\langle \mathrm{VD} \rangle$ is about an order of magnitude weaker than the corresponding advection terms $\langle \mathrm{VA}_e \rangle$ and $\langle \mathrm{VA}_m \rangle$. Hence, to depict the structure of the stretching term, we shall focus on distributions of various terms at the 850-mb level, instead of displaying the vertically averaged patterns. The structure of the advection terms at 850 mb is very similar to that of their vertically averaged counterparts.

The term VA_e exhibits a wavelike structure extending west-northwestward all the way from 165°E to the South China Sea (Fig. 6a). It is evident that VA_e leads the fluctuations in ζ (as inferred from the trough and ridge axes) by approximately a quarter-wavelength. It is the largest term contributing to the vorticity tendency in the southeastern portion of the mean propagation path, where the WP disturbances first become discernible. Similar to the WP vorticity fluctuations (LL, Fig. 16), VA_e is confined mostly below 500 mb, and has a strong west-northwestward tilt with height in the southeastern sector.

An interesting feature in Fig. 6a is that the strongest advection of mean absolute vorticity by the transient fluctuations occurs equatorward of the time-mean monsoon trough axis. (In this study, axes of maximum $\bar{\zeta}$ are used to depict the locations of the mean monsoon troughs, and are marked as bold continuous lines in some of the figures.) The spatial relationship between the extremes of VA_e and the mean monsoon trough axis can best be understood by inspecting the patterns for the advection of mean relative and planetary vorticity by the transient fluctuations (Figs. 6d and 6e). These two advection terms, $\mathbf{V} \cdot \nabla \bar{\zeta}$ and $-v'\beta$, behave very differently on opposite sides of the mean trough axis. To the east of the Philippines, $-\mathbf{V}' \cdot \nabla \bar{\zeta}$ is dominated by the meridional advection of mean relative vorticity, $-(v'/a)(\partial \bar{\zeta}/\partial \phi)$. Equatorward of the monsoon trough axis, both $\partial \bar{\zeta}/\partial \phi$ and β are positive, and $-\mathbf{V}' \cdot \nabla \bar{\zeta}$ and $-v'\beta$ reinforce one another. However, poleward of the mean trough, $\partial \bar{\zeta}/\partial \phi$ becomes negative while β remains positive, and the relative vorticity advection tends to oppose the beta effect. These relationships yield a stronger (weaker) value of $-\mathbf{V}' \cdot \nabla(\bar{\zeta} + f)$ equatorward (poleward) of the mean trough axis, as shown in Fig. 6a. Similar relationships between VA_e and the mean monsoon trough axes are also noted in the Indian and African–Atlantic sectors.

Strong advection of perturbation vorticity by the time-mean flow is found along the axis of maximum mean southeasterlies in the western Pacific, and the axis of maximum southwesterlies in the South China Sea (see Fig. 6b; the time-mean flow structure when WP disturbances are active has been shown in Fig. 17b of LL). The VA_m term is particularly important in the northwestern portion of the mean propagation path, where the disturbances have already developed significantly. Since the axis of maximum mean southeasterlies is situated northward of the mean monsoon trough axis in the western Pacific, VA_m makes a large contribution to the vorticity budget in regions where VA_e happens to be weak.

The stretching term VD also contributes to the WP vorticity balance, mainly in the northwestern portion of the mean propagation path (Fig. 6c). This term is

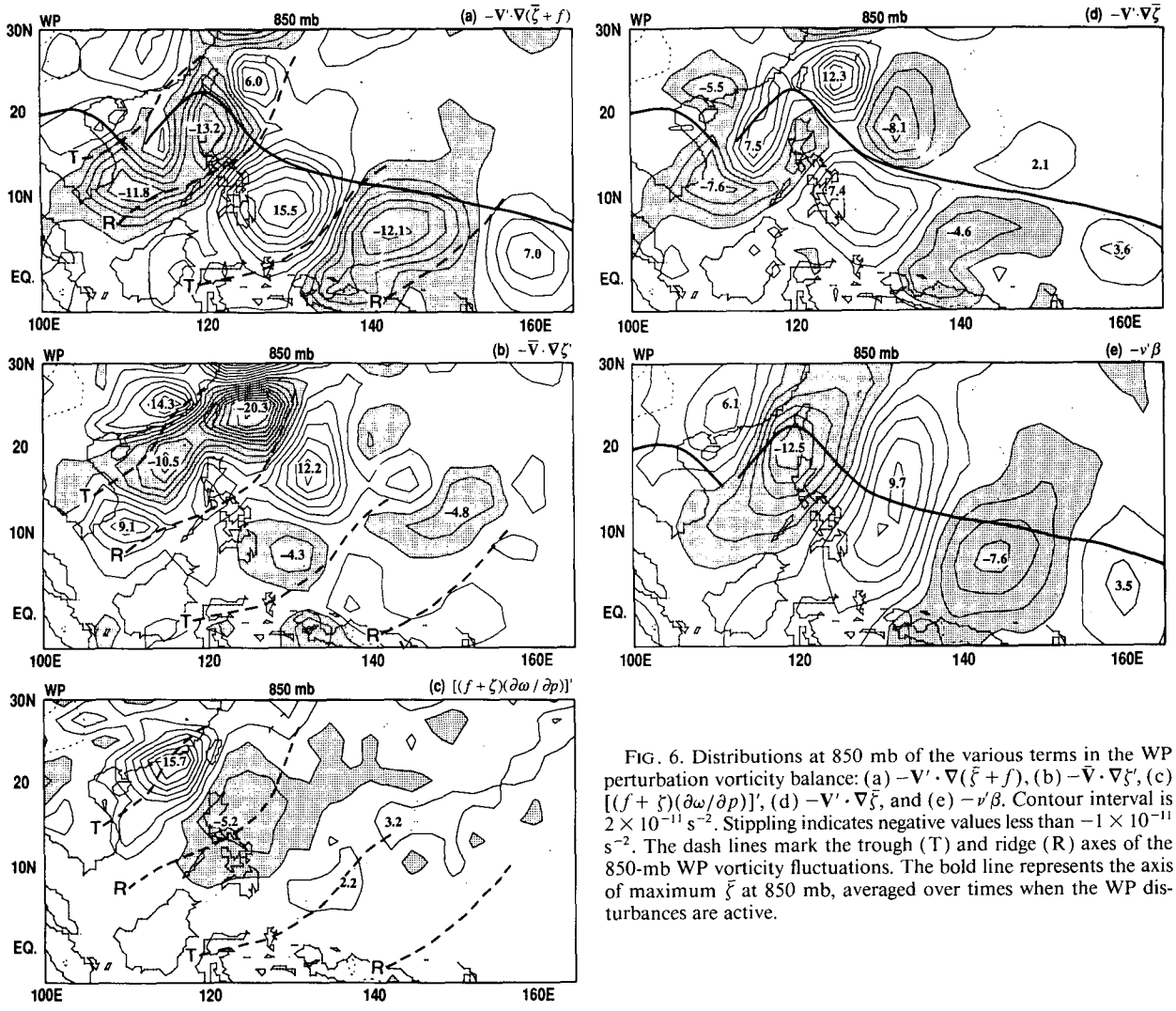

FIG. 6. Distributions at 850 mb of the various terms in the WP perturbation vorticity balance: (a) $-\mathbf{V}'\cdot\nabla(\bar{\zeta}+f)$, (b) $-\bar{\mathbf{V}}\cdot\nabla\zeta'$, (c) $[(f+\zeta)(\partial\omega/\partial p)]'$, (d) $-\mathbf{V}'\cdot\nabla\bar{\zeta}$, and (e) $-v'\beta$. Contour interval is 2×10^{-11} s^{-2}. Stippling indicates negative values less than -1×10^{-11} s^{-2}. The dash lines mark the trough (T) and ridge (R) axes of the 850-mb WP vorticity fluctuations. The bold line represents the axis of maximum $\bar{\zeta}$ at 850 mb, averaged over times when the WP disturbances are active.

dominated by $(f+\bar{\zeta})(\partial\omega'/\partial p)$, that is, the stretching effect associated with the divergent motion in the transient fluctuations. An important distinction between VD and the two advection terms VA_e and VA_m is its spatial displacement with respect to the vorticity fluctuations. The terms VA_e and VA_m lead ζ' by approximately an eighth- to a quarter-wavelength, whereas VD is almost in phase with ζ' below 700 mb and above 300 mb. For sinusoidal disturbances, a forcing that is in phase with the fluctuations contributes to exponential growth, whereas a forcing that is in quadrature with them leads to phase propagation. Hence, the in-phase relationship between VD and ζ' implies that the stretching term contributes rather effectively to the growth of the vorticity fluctuations, whereas the westward phase shift of VA_e and VA_m with respect to ζ' suggests that these advection terms contribute more effectively to the westward propagation.

The 850-mb distributions of VA_e and VA_m for the vorticity balance of the IN disturbances are shown in Figs. 7a and 7b, respectively. Figure 7a shows that VA_e leads ζ' westward by about an eighth- to a quarter-wavelength, implying a westward-propagating tendency of the vorticity fluctuations. Except in northern India, where u' is much stronger than v', strong advection of mean absolute vorticity by the transient fluctuations is found equatorward of the axis of maximum 850-mb $\bar{\zeta}$ (the bold line in Fig. 7). As in the western Pacific, the large (small) amplitude of VA_e equatorward (poleward) of the mean monsoon trough axis is related to the additive (canceling) effects of its two component terms $-v'\beta$ and $-\mathbf{V}'\cdot\nabla\bar{\zeta}$.

The main difference between the vorticity balances in the Indian and western Pacific disturbances is due to the different mean-flow structure in the two sectors. The summertime mean flow in the Indian sector is

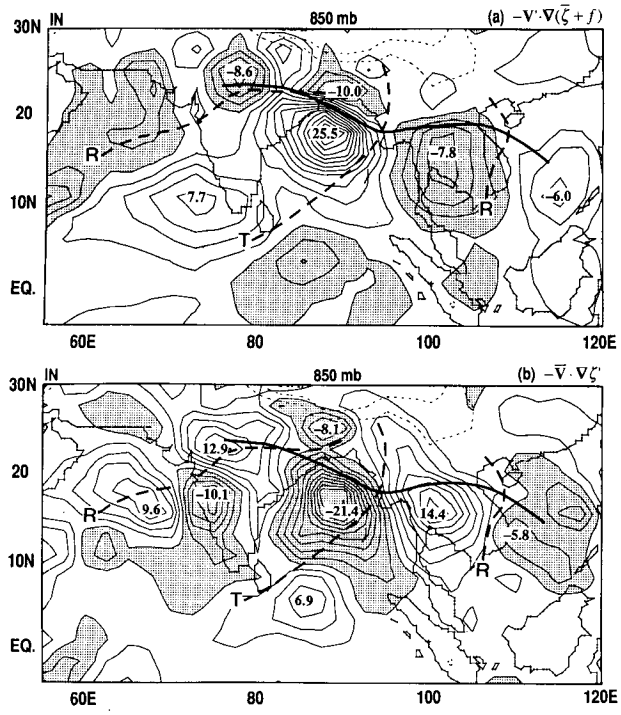

FIG. 7. Distributions at 850 mb of (a) $-\mathbf{V}'\cdot\nabla(\bar{\zeta}+f)$ and (b) $-\bar{\mathbf{V}}\cdot\nabla\zeta'$ for the IN disturbances. Contour interval is 2×10^{-11} s^{-2}. Stippling indicates negative values less than -1×10^{-11} s^{-2}. The dash lines mark the trough (T) and ridge (R) axes of the IN vorticity fluctuations at 850 mb. The bold line represents the 850-mb axis of maximum $\bar{\zeta}$, averaged over times when the IN disturbances are active.

characterized by strong easterlies at the upper levels (not shown) and strong monsoon west-southwesterlies in the lower troposphere (LL, Figs. 2 and 18). The strength as well as the vertical and horizontal shears of the mean flow in the western Pacific are much weaker. Due to the presence of strong low-level westerlies equatorward of the Indian monsoon trough axis, extremes in VA_m are shifted eastward relative to the vorticity fluctuations by an eighth- to a quarter-wavelength at the 850-mb level (Fig. 7b). Hence, VA_m and VA_e are out of phase in the lower troposphere. On the other hand, the strong upper-level easterly flow leads to a westward phase shift of VA_m relative to ζ' above 500 mb, so that VA_m becomes almost in phase with VA_e in the upper troposphere. A net eastward tendency is obtained in the vertically averaged distribution of VA_m (not shown), indicating that the eastward advection by the low-level westerlies is stronger than the westward advection by the upper-level easterlies. The latter finding is mainly a consequence of the stronger ζ' in the lower troposphere. In addition, we also find that the phase lines of both $\langle VT\rangle$ and $\langle VT_c\rangle$ are shifted westward with respect to those of $\langle\zeta'\rangle$. The westward phase shift of $\langle VT_c\rangle$ with respect to $\langle\zeta'\rangle$ implies that the westward tendency associated with $\langle VA_e\rangle$ is stronger than the eastward tendency associated with $\langle VA_m\rangle$. As in the western Pacific, the stretching term is more or less in phase with ζ' in the lower and upper troposphere, and it does not contribute much to the vertically averaged IN mode vorticity balance because of large cancellations between the upper and lower levels.

To illustrate the vorticity balance for the Atlantic disturbances, vertical cross sections of the VA_e and VA_m terms for the AT mode are shown in Figs. 8a and 8b, respectively. It is evident that both VA_e and VA_m are shifted westward relative to ζ' by approximately a quarter-wavelength. We choose to show the vertical cross sections to highlight the enhanced interaction between the upper-level mean flow and the westward-propagating disturbances in the western Atlantic. Figure 8a shows that while VA_e achieves significant amplitude only in the lower troposphere in the eastern part of the Atlantic–African domain, this term becomes quite large in the upper troposphere as the disturbances propagate toward the western Atlantic. Earlier results by Reed et al. (1988) and others also suggest that intensification of Atlantic easterly waves in the western Atlantic may partly be a result of their interactions with the upper-level semipermanent trough in that region.

Figure 8b indicates that the strongest westward mean-flow advection over western Africa–eastern Atlantic occurs at the level of the African midtropospheric easterly current (~600 mb), while the largest VA_m contribution over the central and western Atlantic is located at a slightly lower level (~700 to 850 mb). It

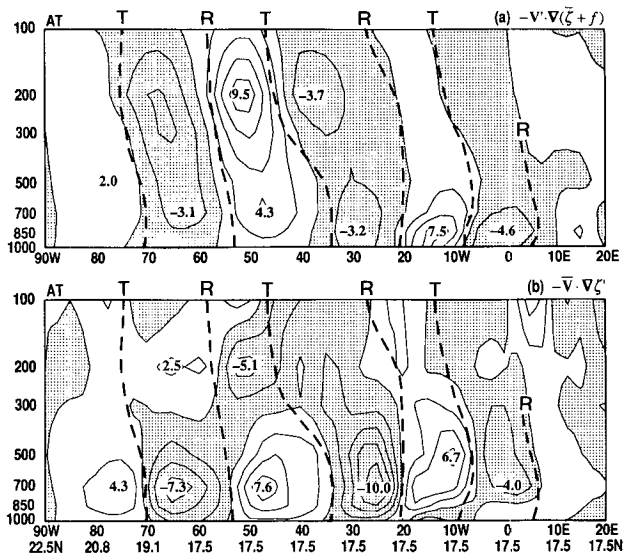

FIG. 8. Vertical cross sections of (a) $-\mathbf{V}'\cdot\nabla(\bar{\zeta}+f)$ and (b) $-\bar{\mathbf{V}}\cdot\nabla\zeta'$ for the AT disturbances. Contour interval is 2×10^{-11} s^{-2}. Stippling indicates negative values less than -1×10^{-11} s^{-2}. The dash lines mark the trough (T) and ridge (R) axes of the AT vorticity fluctuations.

is interesting to note that VA_m is stronger at altitudes where VA_e happens to be weak, so that these two advective effects complement each other in pushing the AT vorticity fluctuations westward. In the vertical average, the two advection terms contribute almost equally to the westward propagation of the AT disturbances throughout the Atlantic domain.

5. Perturbation enstrophy and kinetic energy balance

In this section, we shall evaluate the relative importance of the various dynamical processes in the overall maintenance of the tropical disturbances. The eddy-enstrophy balance of the transient fluctuations will be studied first, so as to obtain a relatively simple picture of the maintenance of the rotational component of the fluctuations. We shall then examine the EKE balances of the dominant tropical modes, and discuss the results in conjunction with the EAPE balances in section 3b, so as to offer a more complete summary of the energetics of the tropical disturbances.

a. *Eddy-enstrophy balance*

The eddy-enstrophy equation may be written as:

$$\underbrace{\frac{\partial \xi_T}{\partial t}}_{\text{NT}} = \underbrace{-\overline{\mathbf{V}'\zeta'}\cdot\nabla(\bar{\zeta}+f)}_{\text{NI}} \underbrace{-\bar{\mathbf{V}}\cdot\nabla\overline{\xi_T}}_{\text{NA}_m} \underbrace{-\overline{\mathbf{V}'\cdot\nabla\xi_T}}_{\text{NA}_e}$$

$$+ \underbrace{\overline{\left[(f+\zeta)\frac{\partial\omega}{\partial p}\right]'\zeta'}}_{\text{ND}} \underbrace{-\overline{\left(\mathbf{k}\cdot\nabla\omega\times\frac{\partial\mathbf{V}}{\partial p}\right)'\zeta'}}_{\text{NC}} + \text{NR},$$

where $\xi_T \equiv \overline{\zeta'^2}/2$ is the eddy enstrophy. The term NT corresponds to the time rate of change of the phase-averaged eddy enstrophy, and is identically zero. The term NI represents the exchange of enstrophy between the mean flow and the transient eddies. The NI term is positive when the eddy vorticity flux is directed down the mean absolute-vorticity gradient. The terms NA_m and NA_e denote the advection of eddy enstrophy by the time-mean flow and the transient fluctuations, respectively. ND and NC correspond to the generation of eddy enstrophy by stretching and tilting effects, respectively, and NR is the residual term. We find that the major terms in the enstrophy balance of the various tropical disturbances are NI, NA_m, ND, and NR. Contributions from NA_e and NC are very weak and will not be discussed.

Vertically averaged distributions of NI, NA_m, and ND for the WP disturbances are shown in Figs. 9a, 9b, and 9c, respectively. Figure 9a shows that eddy enstrophy is being generated (destroyed) by $\langle \text{NI} \rangle$ equatorward (poleward) of the time-mean monsoon trough axis. To understand this distribution, it is useful to separate $\langle \text{NI} \rangle$ into its two component terms $\langle -\overline{\mathbf{V}'\zeta'}\cdot\nabla\bar{\zeta}\rangle$ and $\langle -\beta\overline{v'\zeta'}\rangle$, which are shown in Figs. 9d and 9e, respectively. The pattern of $\langle -\beta\overline{v'\zeta'}\rangle$ is characterized by a strong negative region poleward of the monsoon trough axis (the bold line), and a weak positive region equatorward of it. Since β is a positive-definite quantity, the distribution of $\langle -\beta\overline{v'\zeta'}\rangle$ implies that the meridional eddy vorticity flux is directed poleward to the north of the mean trough axis, and directed equatorward to the south. This configuration of $\overline{v'\zeta'}$, together with the sign reversal of $\partial\bar{\zeta}/\partial\phi$ across the mean trough axis, implies positive generation of eddy enstrophy by $\langle -(\overline{v'\zeta'}/a)(\partial\bar{\zeta}/\partial\phi)\rangle$ on both sides of the mean monsoon trough axis. This inference is consistent with our analysis that $\langle -\overline{\mathbf{V}'\zeta'}\cdot\nabla\bar{\zeta}\rangle$ is predominantly positive. [Note that $-\overline{\mathbf{V}'\zeta'}\cdot\nabla\bar{\zeta} \approx -(\overline{v'\zeta'}/a) \times (\partial\bar{\zeta}/\partial\phi)$, as the meridional gradient of $\bar{\zeta}$ is generally stronger than the corresponding zonal gradient.] In other words, eddy enstrophy is generated as a result of the eddy vorticity flux directed down the mean relative vorticity gradient, and this process tends to reduce the relative vorticity gradient of the time-mean flow. The planetary-vorticity advection is stronger and is largely responsible for the distribution of $\langle \text{NI} \rangle$ shown in Fig. 9a. The enhancement (suppression) of transient activity equatorward (poleward) of the mean trough axis due to the $\langle -\beta\overline{v'\zeta'}\rangle$ term is a feature common to the tropical disturbances identified in all the active sites.

Figure 9b shows that eddy enstrophy is being advected northward across ~20°N from the western Pacific by the time-mean southeasterly flow, and from the South China Sea by the Indian monsoon southwesterly flow. The advection of eddy enstrophy by the mean wind appears to be the dominant process that maintains eddy enstrophy in the northwestern end of the propagation path.

The stretching term VD is the most important process for the *generation* of eddy enstrophy for the WP disturbances (Fig. 9c). The component that contributes most to ND is $\langle (f+\bar{\zeta})(\partial\omega'/\partial p)\zeta'\rangle$, which is related to the convergent (divergent) motion of the fluctuations at the wave troughs (ridges) (i.e., the in-phase relationship between VD and ζ' as noted in section 4). The other noteworthy component of $\langle \text{ND} \rangle$ is $\langle \zeta'^2(\partial\bar{\omega}/\partial p)\rangle$, which is related to the horizontal convergence of time-mean flow $\langle \partial\bar{\omega}/\partial p\rangle$. The latter effect amounts to about a quarter of the amplitude of $\langle \text{ND} \rangle$ in Fig. 9c, and is mostly confined to a band along the mean monsoon trough axis, where the strongest horizontal convergence of the mean flow is located.

The predominantly negative values of the residual term $\langle \text{NR} \rangle$, shown in Fig. 9f, suggest the presence of strong dissipative effects with time scale of a few days. The strongest dissipation is found in the northwestern

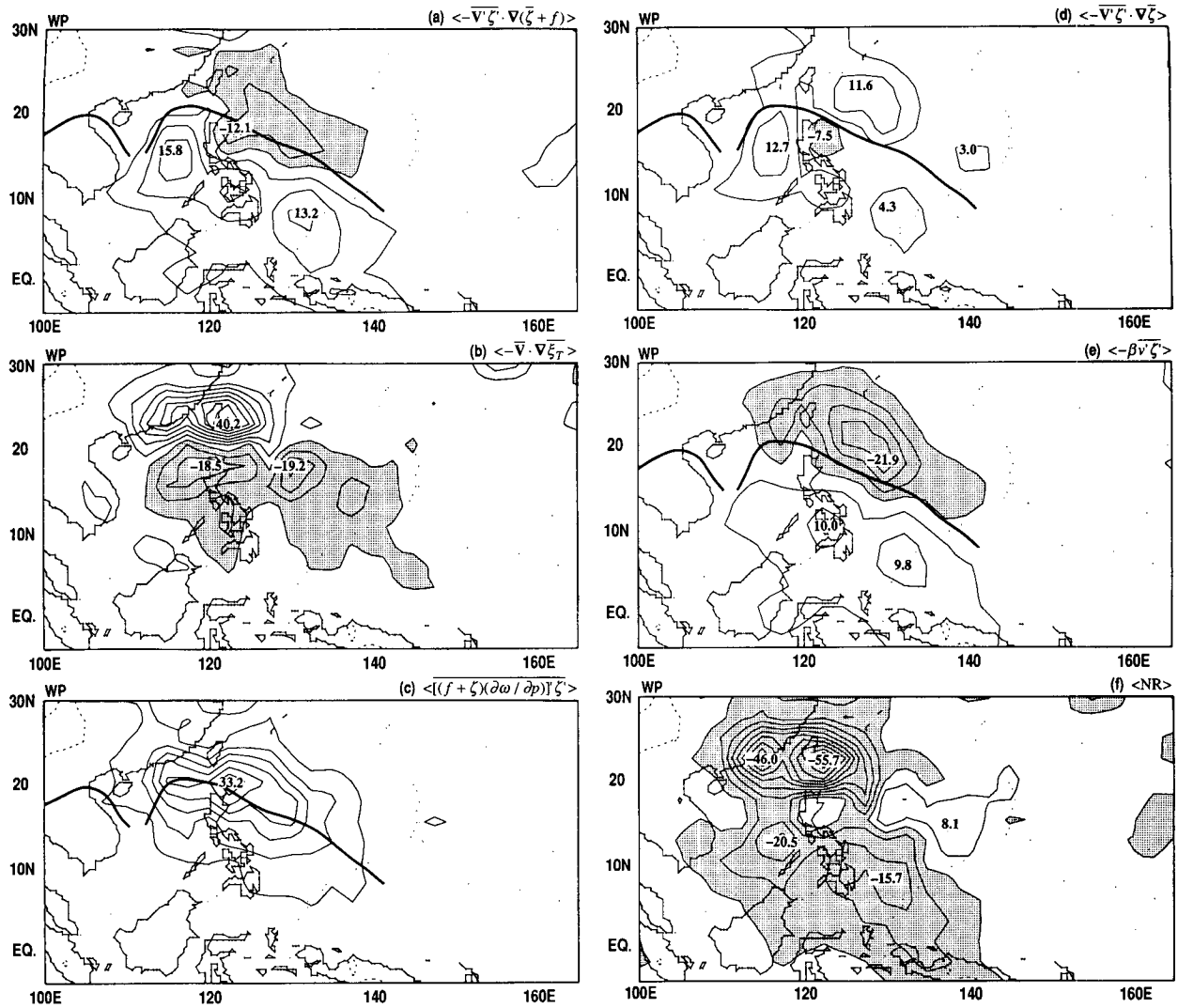

FIG. 9. Vertically averaged distributions of the terms in the WP eddy-enstrophy balance: (a) $-\overline{\mathbf{V}'\zeta'}\cdot\nabla(\bar{\zeta}+f)$, (b) $-\bar{\mathbf{V}}\cdot\nabla\overline{\xi_T}$, (c) $\overline{[(f+\zeta)(\partial\omega/\partial p)]'\zeta'}$, (d) $-\bar{\mathbf{V}}'\zeta'\cdot\nabla\bar{\zeta}$, (e) $-\beta\overline{v'\zeta'}$, and (f) NR. Contour interval is $5\times10^{-17}\,s^{-3}$. Stippling indicates negative values less than $-2.5\times10^{-17}\,s^{-3}$. The bold line represents the axis of maximum $\langle\bar{\zeta}\rangle$.

section of the propagation path near the south China coast. This result is in accord with the earlier finding that ζ' is almost 180° out of phase with VR near this region (section 4). The largest negative values of NR are located at the two lowest levels. Friction is probably responsible for a significant part of the damping near the lower boundary. Weaker dissipation of eddy enstrophy is also found in the upper and middle troposphere, and may partly be a result of subgrid-scale processes such as cumulus convection (section 3).

The main features of the eddy-enstrophy balance for tropical disturbances in the Indian and African–Atlantic sectors are similar to those of the WP disturbances.

b. *Eddy kinetic energy balance*

The eddy kinetic energy balance equation is written as

$$\underbrace{\frac{\partial K_T}{\partial t}}_{\mathrm{KT}} = \underbrace{-[\overline{\mathbf{V}_h'(\mathbf{V}'\cdot\nabla)\mathbf{V}_h'}]}_{\mathrm{KI}} \underbrace{-\bar{\mathbf{V}}\cdot\nabla\overline{K_T}}_{\mathrm{KA}_m} \underbrace{-\overline{\mathbf{V}'\cdot\nabla K_T}}_{\mathrm{KA}_e} \underbrace{-\frac{R}{p}\overline{\omega'T'}}_{\mathrm{KP}} \underbrace{-\nabla\cdot(\overline{\mathbf{V}'\Phi'})}_{\mathrm{KZ}} + \mathrm{KR}, \quad (7)$$

where $K_T \equiv \overline{\mathbf{V}_h'^2}/2$ is the horizontal eddy kinetic energy (EKE), and $\Phi \equiv gZ$ the geopotential. Here, KT, the

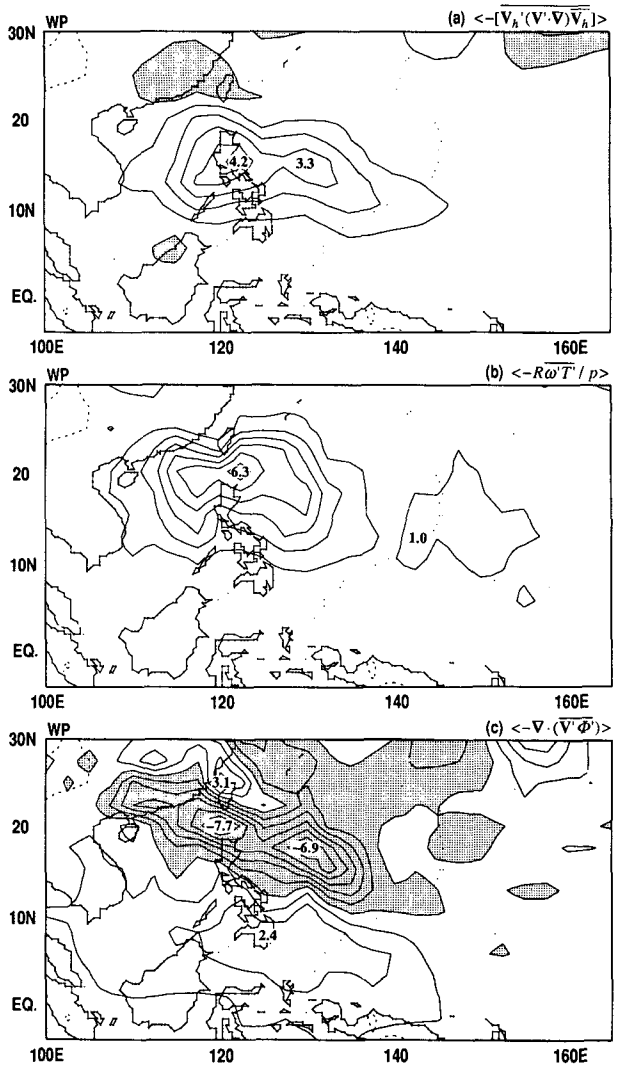

FIG. 10. Vertically averaged distributions of (a) $-[\overline{V_h'(V'\cdot\nabla)V_h'}]$, (b) $-R\overline{\omega'T'}/p$, and (c) $-\nabla\cdot(\overline{V'\Phi'})$ for the WP eddy kinetic energy balance. Contour interval is 1×10^{-5} m^2 s^{-3}. Stippling indicates values less than -0.5×10^{-5} m^2 s^{-3}.

time-rate of change of EKE, is zero. The term KI denotes the barotropic conversion of EKE from time-mean kinetic energy (MKE); KA_m and KA_e represent the advection of EKE by the time-mean flow and the transient fluctuations, respectively. The term KP describes the conversion from EAPE to EKE through the rising (sinking) motion of warm (cold) air parcels. This term also appears in the same form but with opposite sign in the EAPE balance equation (5). KZ represents the generation (destruction) of EKE by local convergence (divergence) of the eddy geopotential flux. Since the KA_m, KA_e, and KZ terms mainly describe the redistribution of energy from one location to another, these terms are often not considered as real sources or sinks. The last term KR represents the net generation or dissipation of EKE by frictional and other subgrid-scale effects.

Vertically averaged distributions of the KI, KP, and KZ terms of the EKE balance for the WP disturbances are shown in Fig. 10, and the corresponding vertical cross sections are displayed in Fig. 11. Figure 10a shows the barotropic conversion of MKE to EKE in the cyclonic-shear zone south-southwestward of the time-mean southeasterly current (LL, Fig. 17b). This result is consistent with the location and the southwest-to-northeast phase tilt of the WP disturbances (LL, sections 4a and 6a). The conversion of MKE to EKE is mainly confined to the atmospheric layers below 500 mb (Fig. 11a), in contrast to the stronger conversion from EAPE to EKE, which occurs almost exclusively above 500 mb (Fig. 11b). The axis of maximum $\langle KP \rangle$ is more or less coincident with the mean trough axis, and is situated slightly (less than 5°) poleward of the axis of maximum $\langle KI \rangle$. Moreover, the distribution of $\langle KP \rangle$ is very similar to that of the stretching term $\langle ND \rangle$ in the eddy enstrophy budget (compare Figs.

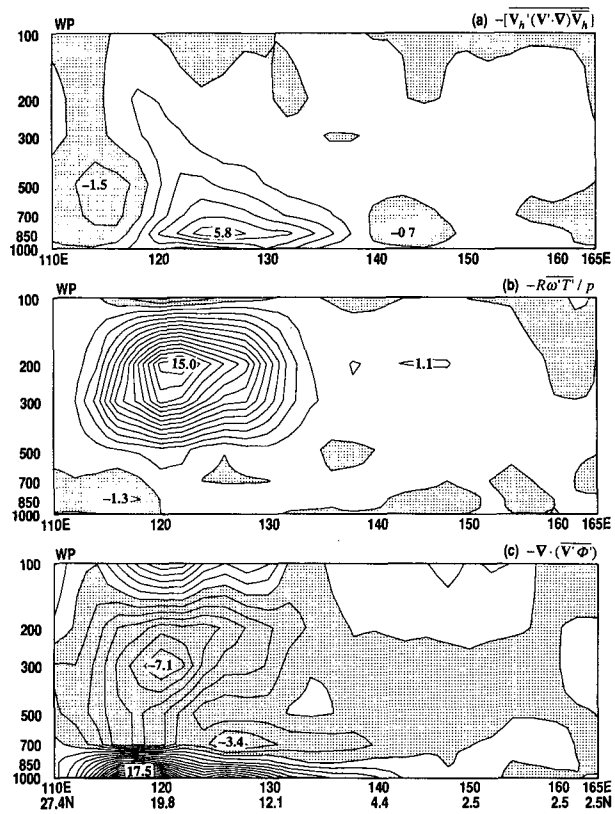

FIG. 11. Vertical cross sections of (a) $-[\overline{V_h'(V'\cdot\nabla)V_h'}]$, (b) $-R\overline{\omega'T'}/p$, and (c) $-\nabla\cdot(\overline{V'\Phi'})$ for the WP eddy kinetic energy balance. Contour interval is 1×10^{-5} m^2 s^{-3}. Stippling indicates negative values.

10b and 9c). This notable resemblance suggests that these two effects are related to the same chain of physical processes: namely, the low-level eddy convergence in the wave troughs (the ND term in section 5a), the diabatic generation of EAPE (the PQ term in section 3b), and the subsequent conversion of EAPE to EKE (the KP term discussed here). The generation and subsequent conversion of EAPE to EKE in the middle and upper troposphere is stronger than the barotropic conversion of MKE to EKE in the lower troposphere, in agreement with our earlier conclusion that latent heating associated with moist convective processes is the most important source of energy for the WP disturbances.

To maintain the balance in (7), the EKE produced by KI and KP has to be destroyed locally, or exported to other regions where it can be destroyed effectively (e.g., through frictional processes near the lower boundary). Such dissipation or transport has to be accomplished by the processes associated with the KA_m, KA_e, KZ, and KR terms. The KA_e term is very small and its contribution is negligible. The net contribution of KA_m is a northward advection of EKE by the time-mean southeasterly flow in the western Pacific, and the mean southwesterly flow in the South China Sea. Compared with the terms KI, KP, and KZ, the magnitude of KA_m is rather small. Hence, the redistribution of EKE has to be achieved by the KZ term, or by unresolved vertical transport associated with the KR term.

Figure 10c shows that a strong reduction of EKE by $\langle KZ \rangle$ occurs along a northwest-to-southeast–oriented zone that is more or less coincident with the axis of maximum production of EKE by the $\langle KP \rangle$ term (Fig. 10b). [Since the computation of KZ entails an accurate determination of the ageostrophic flow, estimates of this term should be viewed with due caution (see also Trenberth 1991).] Positive values of $\langle KZ \rangle$ prevail to the south of this axis of strong eddy geopotential flux divergence. The vertical cross section in Fig. 11c reveals that KZ is responsible for a substantial reduction of EKE between 200 and 500 mb, and for a large increase in EKE below 700 mb, as well as a smaller increase above 200 mb.

To gain some further understanding of KZ, it is useful to rewrite this term as

$$\underbrace{-\nabla\cdot(\overline{\mathbf{V}'\Phi'})}_{\mathrm{KZ}} = -\overline{\mathbf{V}'\cdot\nabla\Phi'} - \overline{\Phi'(\nabla\cdot\mathbf{V}')}$$

$$= \underbrace{-\overline{\mathbf{V}'_h\cdot\nabla_h\Phi'}}_{\mathrm{KZ}_h} \underbrace{-\overline{\omega'\frac{\partial\Phi'}{\partial p}}}_{\mathrm{KZ}_v}.$$

The horizontal component KZ_h describes the change in EKE associated with the eddy motion across the horizontal gradient of Φ', and is strongest in the lower troposphere, where the cross-isobaric component of the horizontal wind perturbations and the horizontal gradient of Φ' are largest. Term KZ_h is predominantly positive since low-level convergence (divergence) tends to coincide with the wave troughs (ridges), so that the ageostrophic component of $\mathbf{V}'_h$ is directed from high to low Φ'. This cross-isobaric flow results in an increase of EKE at the expense of the eddy geopotential energy in the lower troposphere. With weaker wind and geopotential perturbations in the upper troposphere, a smaller generation of EKE by the same mechanism also occurs above the 200-mb level.

In contrast, KZ_v is more important in the middle and upper troposphere, where ω' is stronger. We have shown in LL that for tropical disturbances, rising (sinking) motion is usually found above the low-level wave troughs (ridges), and the strongest geopotential perturbations are located in the lower troposphere (LL, Fig. 16). Hence, the vertical motion above wave troughs and ridges is directed from low to high Φ' against the eddy geopotential gradient, implying an increase in eddy geopotential energy at the expense of the EKE of the transient fluctuations. Recalling the definition of KZ_v, and noting that negative (positive) ω' occurs in association with negative (positive) $\partial\Phi'/\partial p$ above the wave troughs (ridges), it is readily seen that KZ_v is generally negative. Furthermore, since $KZ_v = -\overline{\omega'\partial\Phi'/\partial p} = R\overline{\omega'T'}/p = -\mathrm{KP}$, the conversion from EAPE to EKE in the middle and upper troposphere (KP) is completely offset by the conversion from EKE to eddy geopotential energy (KZ_v). Hence, in association with the geopotential patterns and the three-dimensional circulation of the transient disturbances, the net effect of KZ_v and KZ_h is to redistribute EKE from the upper and middle troposphere (where strong conversion from EAPE takes place through the KP term) to the lower levels. Finally, it is worth noting that KZ_h is actually the pressure-gradient force term in conventional EKE budgets. We have decomposed it into KZ and KP, so as to gain further insight in the large-scale dynamical processes operating in the disturbances.

Figure 12 shows the vertically averaged distribution and vertical cross section of the residual term, KR, for the WP disturbances. The vertical cross section of KR (Fig. 12b) indicates strong dissipation in both the lower and upper troposphere. A similar vertical profile of KR has been reported by Kung (1975) and Kung and Burgdorf (1978) on the basis of EKE budget computations for the tropical western Pacific and eastern Atlantic, respectively. Boundary friction may partly account for much of the dissipation at the lower levels, while cumulus friction or other unresolved subgrid-scale vertical mixing may contribute to the residual in the upper troposphere. From the vertically averaged distributions of K_T (not shown) and KR (Fig. 12a), the time scale of dissipation of EKE near the South China coast is estimated to be approximately 1.5 days.

The vertically averaged distribution and vertical

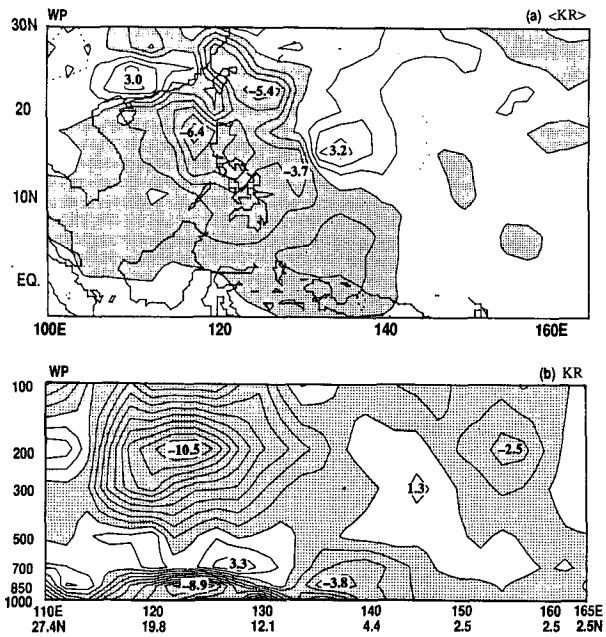

FIG. 12. (a) Vertically averaged distribution of KR for the WP eddy kinetic energy balance. Contour interval is 1×10^{-5} m^2 s^{-3}. Stippling indicates values less than -0.5×10^{-5} m^2 s^{-3}. (b) Vertical cross section of KR for the WP eddy kinetic energy balance. Contour interval is 1×10^{-5} m^2 s^{-3}. Stippling indicates negative values.

cross section of KI for the AT disturbances are shown in Fig. 13. (Corresponding figures for the KP term have been shown earlier in Figs. 3b and 4b.) Figure 13a shows strong positive conversion of EKE from MKE equatorward of the midtropospheric easterly current (at approximately 600 mb along 15°N), in association with the observed southwest-to-northeast phase tilt of the local vorticity fluctuations (LL, Fig. 22a). Along the northern track of the AT disturbances and poleward of the mean easterly current, the horizontal phase tilt of the vorticity fluctuations changes substantially as the disturbances propagate westward. Since KI is related to the horizontal phase tilt of the transient fluctuations, corresponding changes in the barotropic MKE-to-EKE conversion are expected. Positive MKE-to-EKE conversion is observed over western Africa equatorward of 20°N, in association with the southeast-to-northwest phase tilt of the northern disturbances in that region. Farther westward and particularly at mid- and upper levels, the phase tilt along the northern track gradually changes to the same southwest-to-northeast orientation as the southern disturbances, and hence a conversion of EKE to MKE is observed (Figs. 13a and 13b). Away from the midtropospheric easterly current, weaker conversion from MKE to EKE also occurs at upper levels over the Caribbean.

The strongest EAPE-to-EKE conversion for the AT disturbances is found over western Africa–eastern Atlantic, along the northern propagation track. The net contribution of the KP term to the EKE balance for the AT disturbances is larger than that of the KI term (compare Figs. 3b and 13a). As noted in section 3, in association with the strong mean temperature gradients between the Sahara and the cooler eastern Atlantic and equatorial Africa, the EAPE along the northern track in the African–Atlantic region is generated mainly through *baroclinic* conversion of MAPE in the lower troposphere (Figs. 3a and 4a), as distinct from the *diabatic* generation of EAPE by condensation heating in the Indian and western Pacific sectors. Diabatic generation of EAPE by latent heating and subsequent conversion of EAPE to EKE are also found between 200 and 500 mb along the northern track over the central and western Atlantic (Figs. 4b and 4c). However, due to the much weaker temperature and vertical velocity fluctuations over the oceanic areas, the upper-level conversion of EAPE to EKE over the central and western Atlantic is considerably weaker than the lower-level conversion in the eastern Atlantic–western Africa.

Since convective heating appears to be important (section 3), and notable OLR anomalies have been identified for the southern disturbances (LL, Fig. 22), it is interesting to find that the net EAPE-to-EKE conversion along the southern track is rather small (Fig. 3b). To understand this result, we have examined the distributions of ω', T', and KP at all seven pressure levels (not shown). We confirm that there is actually positive EAPE-to-EKE conversion along the southern track, with maximum rates between 200 and 300 mb. However, there is also comparable conversion of EKE

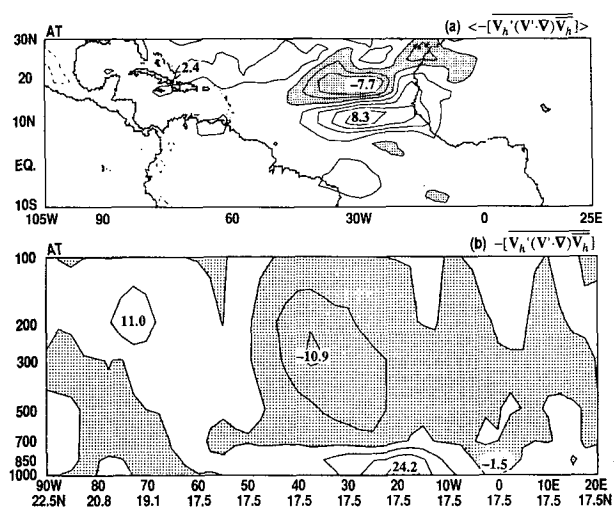

FIG. 13. (a) Vertically averaged distribution of $-[\overline{V_h'(V'\cdot\nabla)V_h'}]$ for the AT eddy kinetic energy balance. Contour interval is 2×10^{-6} m^2 s^{-3}. Stippling indicates negative values less than -1×10^{-6} m^2 s^{-3}. (b) Vertical cross section of $-[\overline{V_h'(V'\cdot\nabla)V_h'}]$ for the AT eddy kinetic energy balance. Contour interval is 5×10^{-6} m^2 s^{-3}. Stippling indicates negative values.

to EAPE below 500 mb. The two effects cancel one another in the column average, leaving a rather small value of $\langle \mathrm{KP} \rangle$ along the southern propagation path. The conversion of EKE back to EAPE is related to the *rising* (*sinking*) motion of lower-level *cold* (*warm*) air parcels above the wave *troughs* (*ridges*). Evaporative cooling in cumulus downdrafts may partly account for the low-level cold cores above the wave troughs, as suggested by many earlier studies (Riehl 1954; Norquist et al. 1977; and others). The dominance of the barotropic conversion from MKE to EKE, as well as the cancellation of the KP term at the upper and lower levels in African waves along the oceanic section of the southern propagation path, have also been noted by Norquist et al. (1977).

6. Summary

By using the composite space–time evolution of transient fluctuations, we have evaluated the relative importance of different dynamical processes in the local heat, moisture, vorticity, enstrophy, and energy balances of the summertime tropical disturbances in the western Pacific, the Bay of Bengal–northeastern India, and the African–Atlantic–Caribbean regions. We find that the westward propagation of these disturbances can mainly be attributed to the advection of perturbation vorticity by the quasi-stationary mean flow and the advection of mean absolute vorticity by the transient fluctuations. Generally, the mean-flow advection of perturbation vorticity is strongest along the axes of maximum mean wind, while the eddy advection of mean absolute vorticity contributes mainly equatorward of the monsoon trough axes. The equatorward shift of the latter feature is a result of the additive (canceling) effects of the eddy advection of planetary vorticity and mean relative vorticity equatorward (poleward) of the mean monsoon trough axes.

Condensation heating associated with cumulus convection is identified as the dominant diabatic heat source for the maritime disturbances in the western Pacific and the Indian monsoon region. The stretching effect and conversion from EAPE (generated by condensation heating) to EKE accompanying moist convection is found to be the most important enstrophy and energy sources for these maritime disturbances. There is also substantial barotropic conversion of kinetic energy from the time-mean flow to the transient fluctuations.

The eddy vorticity flux of the tropical disturbances is usually directed down the mean relative vorticity gradient, resulting in an increase of eddy enstrophy on both sides on the mean monsoon trough. On the other hand, the eddy vorticity flux across the planetary-vorticity gradient leads to a stronger generation (destruction) of eddy enstrophy equatorward (poleward) of the monsoon trough axis. Hence, large conversion of enstrophy from the time-mean flow to the transient fluctuations occurs equatorward of the mean monsoon trough axes, while weak destruction is found poleward of them.

As noted in LL, two preferred propagation paths are discernible in western Africa. The disturbances along the northern track at 20°N are associated with dry desert-type convection that extends only up to 500 mb, much lower than the vertical extent of the moist convection in the maritime disturbances. The stretching effect and conversion from EAPE are still the dominant processes for the generation of eddy enstrophy and EKE in these northern disturbances. However, the EAPE of these disturbances is essentially maintained by the baroclinic conversion of MAPE (as the eddy heat flux is directed down the mean temperature gradient) south of the Sahara Desert. The overall structure and dynamics of the weaker southern disturbances along 10°N are similar to those of the maritime disturbances found in the western Pacific and Indian sectors.

The results of this study and LL suggest that the global four-dimensional products currently archived at various operational weather centers are very useful for the study of tropical synoptic-scale activity. We note that the accuracy of the vertical motion, specific humidity, and mass fields of the ECMWF analyses in the tropics are subject to large uncertainties (Trenberth and Olson 1988; Trenberth 1991). Hence, the results presented here concerning the detailed dynamical balances of the tropical disturbances should be interpreted with such data inaccuracies in mind. Nevertheless, the agreement of many of our findings with earlier results based on other data sources, the correspondence between the calculated diabatic heating fields (Q_1' and Q_2') and the composite OLR distributions, and the similarity between the VT and VT_c terms, provide some consistency checks on our results. Furthermore, Trenberth (1991) has noted that most of the errors in the ECMWF analyses are systematic, so that the anomaly fields may be more reliable than the total fields.

As in most earlier studies on the large-scale dynamics of tropical disturbances, our budget computations are based on composite meteorological fields derived from many individual events. Hence, the findings presented here describe the behavior of the "typical" disturbance in an arithmetically averaged sense. The representativeness of the present results may be assessed by examining the dynamical balances for individual events, and comparing such case studies with the composite picture. These additional analyses may reveal interesting case-to-case differences that are not apparent in our present results.

Since the budget analyses in this study are based on composite mean flow and eddy structure constructed using data for the entirety of the active periods, the present results make no distinction among the growth, mature, and decay stages of the disturbances. It would

be useful to employ compositing techniques suited to identifying the structure of the disturbances and the mean flow during different stages of the evolution of the transient episodes, as was done for extratropical fluctuations by Nakamura and Wallace (1991).

We have noted in LL that there are concurrent changes in the level of synoptic-scale activity and the ambient large-scale flow field. The present study has also illustrated considerable energy and enstrophy exchanges between the transient fluctuations and the mean flow. These findings are indicative of dynamical interactions between the synoptic-scale transient activity and the low-frequency variations of the large-scale flow field. Our understanding of the interactions among tropical phenomena with different time scales is still very limited. By using the EOF temporal coefficients as a measure of the level of transient activity, more systematic and thorough diagnostic studies can be performed to advance our knowledge of the evolution of these tropical disturbances and their interaction with the ambient regional circulations.

Acknowledgments. We would like to thank Y. Kurihara, A. H. Oort, and J. M. Wallace for carefully reading the manuscript and offering helpful comments. The valuable suggestions from L. J. Shapiro and an anonymous reviewer are also appreciated. The figures were prepared by L.-A. Kwan and the Scientific Illustration Group at GFDL. The research of KHL was supported by NSF Grant ATM-8218761, and by NOAA Equatorial Pacific Ocean Climate Studies Program through Grant NA87EAD00039. KHL was also supported by the Joint Institute for the Study of the Atmosphere and Ocean through NOAA Grant NA90AH00073 during the period when the manuscript was finalized.

REFERENCES

Burpee, R. W., 1972: The origin and structure of easterly waves in the lower troposphere of north Africa. *J. Atmos. Sci.*, **29,** 77–90.

——, 1974: Characteristics of north African easterly waves during the summers of 1968 and 1969. *J. Atmos. Sci.*, **31,** 1556–1570.

Carlson, T. N., 1969a: Synoptic histories of three African disturbances that developed into Atlantic hurricanes. *Mon. Wea. Rev.*, **97,** 256–276.

——, 1969b: Some remarks on African disturbances and their progress over the tropical Atlantic. *Mon. Wea. Rev.*, **97,** 716–726.

Kung, E. C., 1975: Balance of kinetic energy in the tropical circulation over the western Pacific. *Quart. J. Roy. Meteor. Soc.*, **101,** 293–312.

——, and H. A. Burgdorf, 1978: Maintenance of kinetic energy in large-scale tropical disturbances over the eastern Atlantic. *Quart. J. Roy. Meteor. Soc.*, **104,** 393–411.

Lau, K.-H., 1991: An observational study of tropical summertime synoptic scale disturbances. Ph.D. thesis, Program in Atmospheric and Oceanic Sciences, Princeton University, 243 pp.

——, and N.-C. Lau, 1990: Observed structure and propagation characteristics of tropical summertime synoptic scale disturbances. *Mon. Wea. Rev.*, **118,** 1888–1913.

Luo, H., and M. Yanai, 1984: The large-scale circulation and heat sources over the Tibetan Plateau and surrounding areas during the early summer of 1979, Part II: Heat and moisture budgets. *Mon. Wea. Rev.*, **112,** 966–989.

Nakamura, H., and J. M. Wallace, 1990: Observed changes in baroclinic wave activities during the life-cycle of the low-frequency circulation anomalies. *J. Atmos. Sci.*, **47,** 1100–1116.

Nitta, T., 1972: Energy budget of wave disturbances over the Marshall Islands during the years of 1956 and 1958. *J. Meteor. Soc. Japan,* **50,** 71–84.

——, and Y. Takayabu, 1985: Global analysis of the lower tropospheric disturbances in the tropics during the northern summer of the FGGE year. Part II: Regional characteristics of the disturbances. *Pure and Appl. Geophys.*, **123,** 272–292.

——, Nakagomi, Y. Suzuki, N. Hasegawa, and A. Kadokura, 1985: Global analysis of the lower tropospheric disturbances in the tropics during the northern summer of the FGGE year. Part I: Global features of the disturbances. *J. Meteor. Soc. Japan,* **63,** 1–19.

Norquist, D. C., E. E. Recker, and R. J. Reed, 1977: The energetics of African wave disturbances as observed during phase III of GATE. *Mon. Wea. Rev.*, **105,** 334–342.

Reed, R. J., and E. E. Recker, 1971: Structure and properties of synoptic-scale wave disturbances in the equatorial western Pacific. *J. Atmos. Sci.*, **28,** 1117–1133.

——, D. C. Norquist, and E. E. Recker, 1977: The structure and properties of African wave disturbances as observed during phase III of GATE. *Mon. Wea. Rev.*, **105,** 317–333.

——, E. Klinker, and A. Hollingsworth, 1988: The structure and characteristics of African easterly wave disturbances as determined from the ECMWF operational analysis/forecast system. *Meteor. Atmos. Phys.*, **38,** 22–33.

Riehl, H., 1954: *Tropical Meteorology.* McGraw-Hill, 392 pp.

Shapiro, L. J., 1986: The three-dimensional structure of synoptic-scale disturbances over the tropical Atlantic. *Mon. Wea. Rev.*, **114,** 1876–1891.

Trenberth, K. E., 1991: Climate diagnostics from global analyses: Conservation of mass in ECMWF analyses. *J. Climate,* **4,** 707–722.

——, and J. G. Olson, 1988: An evaluation and intercomparison of global analyses from the National Meteorological Center and the European Centre for Medium-Range Weather Forecasts. *Bull. Amer. Meteor. Soc.*, **69,** 1047–1057.

Wallace, J. M., and C.-P. Chang, 1969: Spectral analysis of large-scale wave disturbances in the tropical lower troposphere. *J. Atmos. Sci.*, **26,** 1010–1025.

Yanai, M., S. Esbensen, and J.-H. Chu, 1973: Determination of bulk properties of tropical cloud clusters from large-scale heat and moisture budgets. *J. Atmos. Sci.*, **30,** 611–627.